The dynamics of goal-directed rhythmical aiming

Denis Mottet[1,2], **Reinoud J. Bootsma**[1]

[1] Mouvement & Perception (UMR 6559), CNRS & Université de la Méditerranée, 163 avenue de Luminy, CP 910,
13288 Marseille cedex 09, France
[2] Université de Poitiers, Faculté des Sciences du Sport, 4, allée Jean Monnet, 86000 Poitiers, France

Abstract. Based on the kinematics of goal-directed aiming movements in a reciprocal Fitts' task, a minimal limit cycle model is proposed that is capable of producing the behavior observed at levels of task difficulty ranging from 3 to 7. From graphical and statistical analyses of the phase planes, Hooke's planes and velocity profiles, we concluded that the minimal terms to be included in the model were (i) a nonlinear damping in the form of a self-sustaining, velocity-driven Rayleigh oscillator and (ii) a nonlinear stiffness in the form of a softening spring Duffing term. The model reproduced the kinematic patterns experimentally observed in rhythmical precision aiming, accounting for 95% of the variance. The coefficients in the model changed in a systematic way when distance and precision constraints were varied, and the meaning of these changes is discussed in the framework of the dynamical patterns approach.

1 Introduction

Modeling rhythmic human movements as self-sustained oscillators has become an important issue in motor control research (e.g., Haken et al. 1985; Kay et al. 1987, 1991; Kugler and Turvey 1987; Beek et al. 1995, 1996; Kelso 1995; Zaal and Bootsma 1995). A major challenge to this modeling is to identify the nonlinear oscillator components that biological movements may exploit, singly or in combination, to exhibit autonomous limit cycle dynamics. To assess the contribution of the relevant nonlinear damping and stiffness terms, several methods can be used. A good starting point is a topological analysis of the attractive trajectories, seeking graphically for local or global expressions of a typical nonlinearity (Beek and Beek 1988). Such qualitative analyses can be complemented with more quantitative analyses. Time-series methods (spectral or dimensionality analysis) may provide essential information about the nature of the dynamics. Analysis of the global space-time behavior allows identification of the dissipative terms by their effects on the amplitude-frequency and peak velocity-frequency relations (e.g., Kay et al. 1987). Using stability analysis, which is a powerful tool to understanding the transitions between different attractive patterns (e.g., Haken et al. 1985; Buchanan et al. 1997), it is also possible to gain a deeper insight into the transient behavior toward the attractor using perturbation experiments, which is probably the most efficient way to obtain information about the non-conservative terms (Eisenhammer et al. 1991). Finally, one can use statistical methods to quantify the contributions of different nonlinearities (Beek and Beek 1988; Beek et al. 1995) or methods to reconstruct the model more directly from data series (Cremers and Hübler 1987) and even use several of these methods in combination to enhance the precision of the modeling (e.g., Bingham et al. 1991; Beek et al. 1996).

It is well known that in precision aiming, time and space relate in a systematic fashion (e.g., Woodworth 1899; Fitts 1954), leading to speed-accuracy trade-offs whose underpinnings are to date still subject to debate (e.g., Meyer et al. 1988; Plamondon and Alimi 1997). Broadly speaking, these speed-accuracy trade-offs imply that any experimental increase in relative precision requirements will lead to a systematic drop in average speed, accompanied by systematic changes in movement kinematics (e.g., longer decelerative phase for narrow targets, time to peak velocity scaling to movement amplitude; MacKenzie et al. 1987). The question of how time and space relate is also central to modeling the dynamical properties of unconstrained rhythmical movement (e.g., Kay et al. 1987), where the systematic drop in amplitude that occurs with an increase in movement frequency is explained using a hybrid model combining Rayleigh and Van der Pol dissipation. However, few studies have addressed the question of how time and space relate in precision aiming from a dynamical systems perspective (but see Schmidt et al. 1995; Mottet and Bootsma 1995).

Correspondence to: R.J. Bootsma
(e-mail: bootsma@laps.univ-mrs.fr, Fax: +33-4-91172252)

In this article, the fundamental question of how distance and precision constraints influence the dynamics of upper arm aiming is addressed. Given the general assumption that rhythmical precision aiming motion (as produced in a Fitts' task) is a self-sustained oscillation in which the frequency and the stability are adapted to cope with the (relative) precision requirements of the task, our aim is to propose a minimal dynamical model capable of reproducing the observed behaviors and the changes in kinematics that occur with the changes in required precision.

The article is organized as follows. In Sect. 2, a method is proposed for identifying the oscillator components, assembled to produce the rhythmic precision aiming movements. The experimental method is described in Sect. 3, and the results of data analysis and modeling are detailed in Sect. 4. Finally, we highlight several important results and new routes opened by this experiment in the Discussion.

2 Modeling strategy and assumptions

As a starting point, the method assumes that the action system relies on limit cycle dynamics to produce rhythmic movements in an abstract task space (Saltzman and Kelso 1987) and that a graphical and mathematical analysis of the observed kinematics can reveal the assembled oscillatory components giving rise to the limit cycle regime. Second, we assume that the attractor does not change at the time scale of observation, that the time of observation is much longer than the relaxation time toward the attractor, and that stochastic fluctuations at a micro-scale level express themselves as random noise, pushing the observed behavior around the average attractive dynamic pattern. These assumptions are widely accepted (e.g., Haken et al. 1985; Kay et al. 1987; Schöner and Kelso 1988a,b; Schöner 1990; Beek et al. 1995), even if higher-order dimensional systems might better account for the supposed random noise around the limit cycle (Mitra et al. 1997). Our method combines qualitative graphical analyses to identify the nonlinear functions underlying rhythmic precision aiming and quantitative statistical procedures to assess how their respective contributions change with distance and precision requirements.

The first step is to obtain some insight into the oscillator components, which can be done by visual inspection of graphical representations of the data. From the many possible representations, three were selected. First, a phase plane representation (position vs velocity) is a classical tool, useful for getting an idea of the level of nonlinearity of the underlying oscillatory process. Every deviation from a circle is a consequence of nonlinearity, mainly due to the dissipative components, which express themselves in the stability. Second, a Hooke's plane representation (position vs acceleration) allows a direct assessment of the stiffness function (Guiard 1993). Stiffness is the k parameter in the equation $\ddot{x} - kx = 0$. Hence, the global stiffness is equivalent to the general slope of the portrait. However, more interesting are

probably the local stiffness (given by $k = \ddot{x}/x$ for every point on Hooke's portrait) and the local stiffness changes represented by the changes in this ratio. Third, the velocity profile (velocity vs time) was chosen as the best and most well-known representation including time. It was included here as a key element because this representation allows precise assessment of the time behavior of the data and model and because extensive work has been done on the bell-shaped velocity profile in aiming movements (e.g., Atkeson and Hollerbach 1985; Plamondon and Alimi 1997).

The second step is to assess the respective contribution of the nonlinear components thus identified, which can be done using multiple linear regression. However, in order to be able to compare the absolute value of the coefficients obtained through statistical regression, a normalization of the data must be performed. To this end, the spatial dimension of the data is rewritten in units of maximal deviation from the center of oscillation, and the time dimension of the data is rewritten in units of cycle time.

From the assumption that the motion results from second-order dynamics with a fixed origin, fixed mass, and fixed main frequency, the general equation of motion reads:

$$\ddot{x} + F(x, \dot{x}) = 0 \tag{1}$$

where x is the normalized spatial deviation from the origin, the dot represents differentiation with respect to normalized time, and the F function summarizes the linear spring plus the contribution of all the (conservative and dissipative) nonlinear components of the motion. Obviously, F can be computed from movement data, thus allowing regression of the components of the model toward $\ddot{x}$ using multiple linear regression. The method described here is similar to the W method (Beek and Beek 1988), which has proven to be a valuable tool in revealing the individual contributions of the nonlinear terms in juggling (Beek and Beek 1988; Beek 1989), pendulum swinging (Beek et al. 1995), or rhythmic forearm movements (Mottet 1994). The original W method uses stepwise regression of all the possible terms in W, up to a combined power of 3 (i.e., x, x^3, $\dot{x}$, $x^2\dot{x}$, $x\dot{x}^2$, $\dot{x}^3$, see Beek and Beek 1988). Such a procedure did not yield useful results with respect to the present data set. The regression process led to an unstable model for 93% of the individual trials and included a significant linear damping in only 10% of the cases. This disappointing result is due to the lack of sign constraints on the coefficients in the regression process: If the result is to be a self-sustaining oscillator, the linear damping must be negative, while at least one of the nonlinear damping terms must be positive. Consequently, our method starts with qualitative graphical analyses to identify the nonlinear terms to be included in the model. Once the model is identified, we use multiple linear regression to assess how the contributions of the different terms change with distance and precision requirements.

3 Experiment

3.1 Task, procedure, and experimental design

The subjects were nine volunteers (two women and seven men, aged 21–36 years). None suffered from any known motor impairment of the dominant arm (two were left-handed). All participants had normal or corrected to normal vision.

The task was to perform as many back and forth movements as possible in 15 s between two targets printed on a model sheet. Each target consisted of an elongated tolerance zone, centered on a 1 mm cross. If the error in any single trial was more than 5%, or if the subject produced more than two consecutive trials with 0% error, the trial was rerun with the injunction to adjust the speed.

The recording system consisted of an Océ Graphics G6453 digitizing tablet connected to a Macintosh PowerBook computer. This tablet can read the position of a nonmarking stylus pen input device within a distance of 2.5 mm from its surface. It provides two-dimensional position coordinates at a rate of 163 Hz with a spatial accuracy better than ± 0.5 mm.

At the start of each trial, a model sheet (A4) was fixed on the digitizing tablet that rested on a tabletop. Subjects were allowed to modify the tablet orientation at their convenience within a range of about 30°. All the subjects chose an orientation allowing the forearm to be roughly parallel to the vertical axis of the model sheet. A trial started with an initial pointing at the two target centers, to calibrate the system. Then, the subjects were instructed to begin the trial. When they felt they were complying with the constraints (i.e., going as fast as possible with less than 5% error), they informed the experimenter, who started the recording about 1 s later. The subjects were instructed to continue their movement until 15 s had elapsed and the computer sounded a bell. At the end of each trial, information about performance was provided (total number of target hits, error for each target).

Each subject performed a total of 25 trials in one experimental session with the order of conditions being randomized. The 25 trials per subject resulted from a two-factor experimental design with repeated measures on the amplitude of movement (D: 80, 120, 160, 200, and 240 mm) and the target size or endpoint tolerance (W: 4, 8, 12, 16, and 20 mm). Computing the task's index of difficulty (Fitts 1954), the design gave rise to a single experimental factor with 18 levels (i.e., $ID = \log_2(2D/W)$: 3.00, 3.32, 3.58, 3.74, 3.91, 4.00, 4.32, 4.58, 4.64, 4.74, 4.91, 5.06, 5.32, 5.64, 5.91, 6.32, 6.64, 6.91).

3.2 Data reduction

From the bidimensional data sampled by the graphics tablet, only the relevant axis was processed. Here, following the task-dynamic approach (Saltzman and Kelso 1987), the method assumes that the rhythmical planar movement in Fitts' task reduces to a one-dimensional task space (the task's main axis, linking one target center to the other).[1]

The position time series were filtered at a cut-off frequency of 10 Hz with a dual-pass, second-order Butterworth filter. From the filtered data, the first and second time derivatives were computed using the first central difference technique.

Every individual trial was finally summarized in an average normalized cycle. This normalized average cycle is taken to represent the dynamical organization (i.e., the limit cycle) that emerged in response to the task demand, the stochastic noise from the micro-scaled fluctuations being canceled out through the averaging process. The average cycle computation involved the following steps. First, the time series recorded during a 15-s trial were segmented into half-cycles representing the motion from one target to the other, as in Fitts' (1954) original paradigm. On average, a 15-s trial consisted of 15.9 full cycles, with a minimum of 5 and a maximum of 55 depending on the task difficulty. Each half-cycle was subsequently normalized using 21 (time) equidistant points, and the normalized half-cycles beginning at the same target were averaged point by point. Finally, combining the back and forth normalized average half-cycles gave the (42 points) normalized average cycle. This normalized average cycle, which is supposed to represent the attractive pattern governing the dynamics of the end effector on the task's main axis, served as a basis for all graphical and statistical analyses.

4 Data analysis and modeling

4.1 Graphical analysis

In this section, the analysis focuses on Hooke's portraits of the data, using phase planes and velocity profiles as complementary representations. Figures 1, 2 and 3 show the data portraits obtained for the 25 experimental conditions (phase portraits, Hooke's portraits, and velocity profiles, respectively). All these data are plotted in the normalized space previously defined, where the scales of position, velocity, and acceleration are comparable. For example, for a pure linear process, the scale is unity in every dimension (i.e., $x_{\max} = \dot{x}_{\max} = \ddot{x}_{\max} = 1$), and the harmonic nature of the dynamics leads to a phase portrait on the trigonometric circle, a Hooke's portrait as a straight line, and a velocity profile as a perfect sinusoid.

Starting with a general inspection of the Hooke's portraits in Fig. 2, the most striking aspect is the general tendency to deviate from a straight line which clearly appears both with increasing aiming distance (Fig. 2: top to bottom) and decreasing target width (Fig. 2: left to right). Because a linear (harmonic) oscillator implies a straight line in Hooke's plane, this tendency reflects the increasing influence of nonlinear terms in the data with

---

[1] This choice is reinforced by the fact that the little movement that did occur along the ignored dimension (1.7 cm on average) was independent of task conditions (distance and target width).
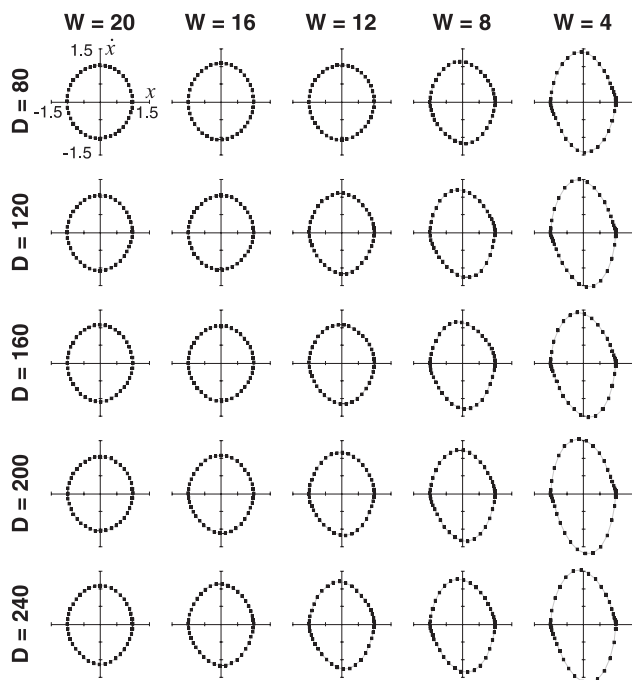
Fig. 1. Average normalized phase portraits for the 25 experimental conditions. Increasing distance (*top to bottom*) and decreasing target width or tolerance (*left to right*), combining in increasing *ID* (*top-left to bottom-right*), produces systematic deviations from a circle (harmonic motion). Increased skewing to the second and fourth quadrants denotes the operation of a Rayleigh-type dissipation, nonhomogeneous distribution of the points denotes a slowing down when arriving at the targets, and increasing maximal velocity denotes a stronger nonlinear behavior
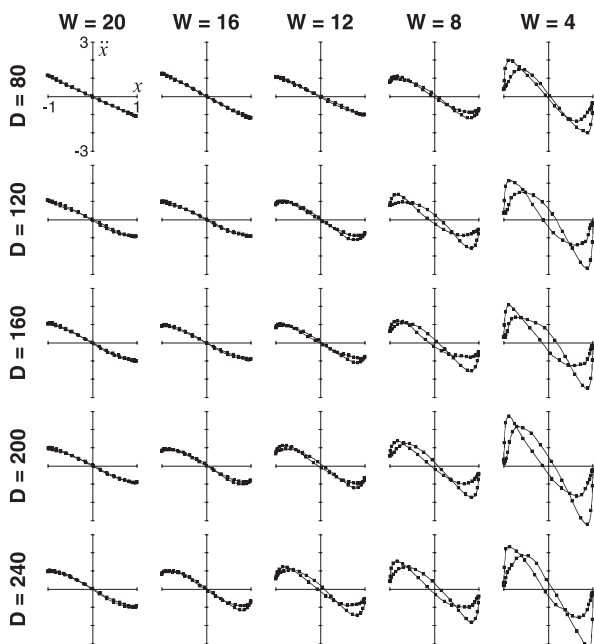
Fig. 2. Average normalized Hooke's portraits for the 25 experimental conditions. Increasing distance (*top to bottom*) and decreasing target width or tolerance (*left to right*), combining in increasing *ID* (*top-left to bottom-right*), produces systematic deviations from a straight line (harmonic motion). Hooke's portrait exhibits (i) an increasing N shape denoting a softening spring and (ii) within each half-cycle, an increasing asymmetry denoting a Rayleigh-type damping (see Fig. 4)
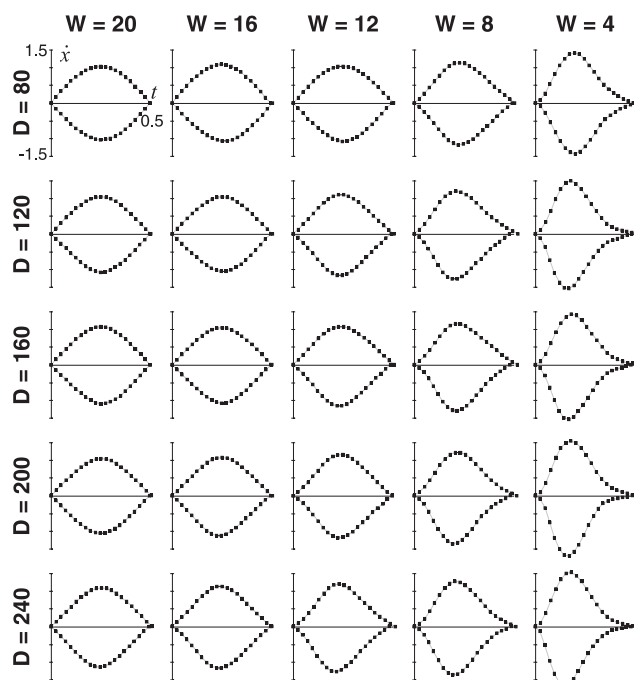
Fig. 3. Average normalized velocity profiles for the 25 experimental conditions. Increasing distance (*top to bottom*) or decreasing tolerance (*left to right*), combining in increasing *ID* (*top-left to bottom-right*), leads to more asymmetric velocity profiles, with maximal velocity attained in the early part of the motion

the increase in task difficulty. To quantify this effect, we introduce a simple measure of the relative contribution of the nonlinear terms in the observed motion. From both (1) and Hooke's portraits, it is clear that the amount of variance that can be attributed to simple harmonic motion can be measured by the r^2 of the linear regression of position onto acceleration. The residue of this regression measures the influence of the sum of all the nonlinear terms (as does the W function in Beek and Beek 1988). Hence, the percentage of variance that is to be attributed to nonlinear components can be assessed using $1 - r^2 = $ NL. Using NL as a dependent variable, a two-way ANOVA showed an increase of NL with distance ($F(4, 32) = 21.82$, $P < 0.0001$, Effect Size $ES = 4.81\%$) and a decrease with target width ($F(4, 32) = 197.61$, $P < 0.0001$, $ES = 72.60\%$), with no significant interaction. The contribution of nonlinear terms was also found to increase with task difficulty ($F(4, 32) = 82.57$, $P < 0.0001$, $ES = 82.51\%$).

4.2 Model proposition

From the analysis of the data in Fig. 2, we concluded that the harmonic process for the lowest *ID* (*NL* = .00) became strongly nonlinear for higher *ID*s (*NL* = .54). Hence, Hooke's portrait for the higher *ID*s should be rich in information about the conservative and dissipative nonlinear terms to include in the model (see also the simulation in Fig. 4).
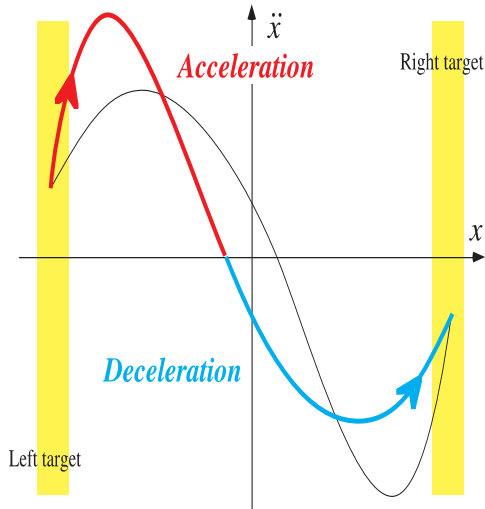
Fig. 4. Typical Hooke's portrait for a high *ID* obtained from numerical simulation with the RD model. The path from the left to the right target is in *bold* (the return *thin*). The acceleration phase is depicted *dark gray* and the deceleration phase in *light gray*. The portrait tends to an N shape, but the profile is asymmetric with (i) a peak acceleration greater than the peak deceleration and (ii) zero acceleration (peak velocity) reached in the first part of the motion. The asymmetry of the acceleration profile in a half-cycle is a classical result in pointing research, the acceleration phase being shorter and sharper than the deceleration phase (MacKenzie et al. 1987)

The shape of this Hooke's portrait can be considered the best graphical representation of the stiffness in both a local and a global view, thus providing valuable information on the nature of the stiffness function. From Fig. 2, it is easily appreciated that Hooke's portrait tends to an N shape with increasing *ID*. This N shape indicates that the local stiffness decreases as the system gets closer to the targets (Fig. 4), which is characteristic of a softening spring behavior. Thus, a negative x^3 is to be included in the equation of motion, which becomes that of a cubic softening Duffing oscillator:

$$\ddot{x} + x - x^3 = 0 \qquad (2)$$

Gaining insight into the nonconservative damping terms is not as straightforward. Focusing again on the Hooke's planes (Figs. 2 and 4), one notes that with only Duffing terms, the positive and negative parts of a half-cycle would have been identical, which is obviously not the case when *ID* is high. This asymmetry within a half-cycle[2]. (Fig. 4) can be achieved with the inclusion of dissipative terms which ensure that (i) the absolute value of peak acceleration is larger than that of deceleration

and (ii) that peak velocity is reached in the first part of the half-cycle, thus leading to phase portraits skewed to the second and fourth quadrants (e.g., see Fig. 1 for $D = 240$ and $W = 4$). Moreover, the sign of the linear damping must be opposite to the sign of nonlinear damping, with a negative linear damping to obtain a limit cycle. The simplest oscillator that fulfills these requirements was first described by Lord Rayleigh for pipe organs. Hence, a Rayleigh term ($\dot{x}^3$) must be included in the equation of motion:

$$\ddot{x} + x - \dot{x} + \dot{x}^3 = 0 \qquad (3)$$

Thus far, the graphical analysis conducted has ascertained that the minimal terms to be included in the equation of motion were (i) a dissipative term leading to a Rayleigh self-sustaining oscillator (3) and (ii) a conservative term leading to a softening Duffing stiffness (2). In the normalized space defined previously, the equation of this minimal model (RD model in the following) reads:

$$\ddot{x} + c_{10}x - c_{30}x^3 - c_{01}\dot{x} + c_{03}\dot{x}^3 = 0 \qquad (4)$$

where the dot represents differentiation with respect to normalized time, x the spatial deviation from the origin in the normalized space, and the coefficients are indexed following the *W* method notation where c_{ij} denotes the coefficient of $x^i\dot{x}^j$.

The fit of the RD model to the data recorded in the experiment was explored using statistical regression methods. All the regressions were based on (4) using multiple linear regression of all the RD model's terms (i.e., x, x^3, $\dot{x}$, $\dot{x}^3$) onto $\ddot{x}$ to obtain an estimate of the coefficients (respectively, c_{10}, c_{30}, c_{01}, c_{03}). For the 225 normalized average cycles, these regressions revealed that the model accurately predicts the observed behavior, accounting for 95% of the variance on average. The best fit was obtained for the most harmonic trials (100% of the variance for $D = 80$ and $W = 20$), while the lowest fit was obtained for the trials with the highest *ID*s, where the left-right and right-left movements were somewhat different (82% of the variance for $D = 200$ or 240 and $W = 4$). These results confirm that the RD model, while including only four parameters, can adequately capture the dynamic behavior of the end-effector in rhythmical precision aiming (Fig. 5), allowing us to address the question of the changes in parameters with the changes in distance and precision.

5 Effects of task constraints on the coefficients in the model

In the previous section, the contribution of the nonlinear terms was found to increase with *ID*, and we proposed a minimal dynamical model that adequately captures this dynamic behavior. The issue to be addressed in this section concerns the influence of the task constraints on the contribution of the Rayleigh and Duffing components, which is difficult to estimate from graphical representations and will be addressed through the

---

[2] It is important to distinguish the asymmetry that may be observed between left-right and right-left movements (i.e., between peak acceleration in the first half-cycle and peak deceleration in the second half-cycle) from the asymmetry to be observed within half a cycle. The former (e.g., Fig. 2 for $D = 240$ and $W = 4$) suggests a difference between extension and flexion movements, while the latter points to a difference between acceleration and deceleration phases that are also evident in the deviation from a symmetrical bell-shape in the velocity profile (Fig. 3).

Fig. 5. Hooke's portraits obtained by numerical simulations with the RD model for the 25 experimental conditions. These simulated Hooke's portraits fit the experimental data in Fig. 2 with an average $r^2 = 0.95$

analysis of the changes in the damping and stiffness coefficients. A primary analysis in the normalized space, where all coefficients in the RD model are comparable, is useful to clearly quantify and point out the main topological aspects. A subsequent analysis in absolute physical time and space will complete the investigation, addressing the question of the time behavior in relation to the spatial constraints.

5.1 Topological aspects

Because the absolute distance or target width no longer appear in the normalized space, the analysis of the contribution of the Duffing and Rayleigh terms in the nonlinear behavior of the oscillator is better addressed when collapsing the D and W factors in a measure of the task's difficulty. The influence of the ID on the values of the coefficients in the RD model was found to be significant for both the Duffing and the Rayleigh terms. The results of the analysis of variance (ANOVA) are summarized in Table 1, and the ID effect is illustrated in Fig. 6.

The conservative linear and cubic Duffing coefficients exhibit a roughly parallel increase when task difficulty increases (Fig. 6). Therefore, the roots of the stiffness function move inward, and the amplitude of the oscillation covers an increasing part of the inter-root distance. Using $S = 1/\sqrt{c_{30}/c_{10}} \times 100\%$ as a measure of the percentage of the inter-root distance covered by the (normalized amplitude of the) oscillation, we found that S increased from 7% to 99% with ID. Hence, increasing

Table 1. Results of the analysis of variance (ANOVA) on the coefficients of the RD model in normalized time and space. For each experimental factor, the F value and effect size (ES = the amount of variance explained) of the effect is reported. The significance of the F values was determined after Greenhouse and Geiser correction. The effects of distance, target width, and ID were significant ($P < 0.05$) for the four coefficients in the RD model, but no interactions reached significance

	Target width effect		Distance effect		ID effect	
	$F(4,32)$	ES (%)	$F(4,32)$	ES (%)	$F(17,136)$	ES (%)
c_{10}	57.99	62.00	17.23	4.07	37.90	70.46
c_{30}	68.65	62.59	18.11	4.42	41.08	71.20
c_{01}	30.85	54.94	6.50	2.20	20.37	62.44
c_{03}	43.93	50.40	4.00	2.48	15.24	56.83

task difficulty clearly makes the stiffness act more as a softening spring, with the roots of the stiffness function moving toward the targets, and the oscillation running along the entire inter-root distance for the highest ID. A major consequence of this change in stiffness is a local change in angular frequency due to the decreased stiffness in the neighborhood of the targets. As the time normalization was performed using the actual frequency of the oscillator (i.e., the experimentally recorded frequency Ω), the local slowing down (due to the increase of the cubic Duffing coefficient c_{30}) is compensated by an increase in the linear stiffness coefficient c_{10}. When c_{10} is higher than unity, this detuning (Beek and Beek 1988) indicates that the nonlinear stiffness makes the system run slower than its eigenfrequency (i.e., $\omega_0^2 = c_{10}\Omega^2$), which clearly points out the nonlinear nature of this slowing down.

The dissipative damping coefficients also exhibit a roughly parallel increase when task difficulty increases. All the individual trials (except 2 out of 225 that rendered pure harmonic processes) exhibited the required sign opposition. For ID higher than 4, the system exhibited a more and more stable Rayleigh limit cycle
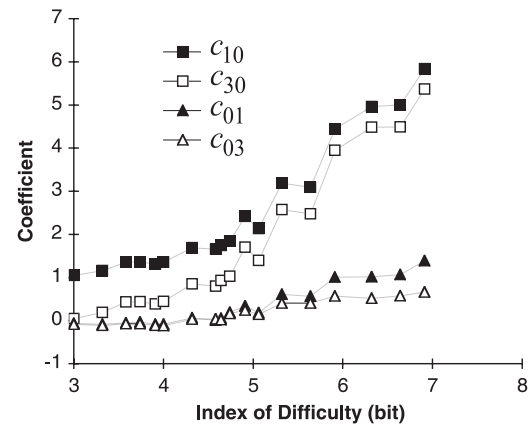
Fig. 6. Coefficients of the RD model (normalized time and space) as a function of task difficulty. Increasing ID shows a parallel increase of the damping (*triangles*) and stiffness (*squares*) coefficients, denoting an increasing contribution of the nonlinear terms

regime (Fig. 6) with increasing positive values for c_{01} and c_{03} [remember that c_{01} is preceded by a minus sign in (4)]. For *ID* lower than 4, the value of the dissipative c_{01} coefficient was relatively small but negative, which indicates that the system behaved in a quasi-harmonic fashion, but as an unstable, repelling Rayleigh limit cycle. This point will be discussed later. Overall, the increase in the value of the linear damping coefficient c_{01} indicates that the stability of the system increased with *ID*.

To summarize, the general increase in the absolute value of the coefficients with *ID* denotes the rising influence of the nonlinear terms on the limit cycle behavior of the system. On the one hand, the system slows down in the neighborhood of the targets, due to the increase in the stiffness coefficients. On the other hand, the system behaves in an increasingly stable way due to the increase in the damping terms. However, the higher coefficients for the stiffness terms indicate that their relative contribution is stronger than that of the damping terms. It is finally worth noting that all the terms in the RD model participate in the increase of the nonlinear behavior with *ID*, thus clearly showing that the RD model is minimal in terms of the dynamical components to be included.

5.2 Time and accuracy aspects

The analysis previously conducted in normalized space allowed us to address the main topological aspects of rhythmical aiming, showing an *ID* effect on the value of all the coefficients in the RD model. Reintroducing the observed frequency Ω and the maximum deviation from the center of oscillation A in the coefficients of (4), it is possible to compute the value of the non-normalized coefficients (i.e., $C_{01} = c_{01}\Omega$, $C_{03} = c_{03}/\Omega A^2$, $C_{10} = c_{10}\Omega^2$, $C_{30} = c_{30}\Omega^2/A^2$), thus switching back the analysis to absolute physical metrics in both space and time. In absolute time-space metrics, the analysis can address the time behavior of the system in relation to the task's spatial requirements. Moreover, the effects of the distance and target width are no longer collapsed in their ratio. Hence, the analysis can make the distinction between the effects of the distance and target width factors on the values of the absolute coefficients in the

RD model. The results of the ANOVA performed on the absolute coefficients and movement times are summarized in Table 2.

In line with the literature on Fitts' task, the time behavior of the system was influenced by the distance and target width factors: The movement frequency increased for shorter distances and larger target widths, without significant interaction. Using the same measures as Fitts (1954), the half-cycle duration (movement time, *MT*) was found to increase with task difficulty, and averaged over subjects, Fitts' law explained 93% of the observed variance ($MT = 0.249 * ID - 0.623$, $F(1, 16) = 227.04$, $P < 0.0001$). To account for these changes in frequency with distance and target width, the conservative linear stiffness coefficient C_{10} increased with target width and decreased with distance, without significant interaction (Fig. 7A). Conversely, the softening Duffing coefficient C_{30} increased with decreasing target width and distance, with a stronger effect of target width for shorter distances (Fig. 7B). These results indicate that the adaptation of the overall speed to the distance and accuracy constraints implied a systematic evolution of the two stiffness coefficients. The increase in *MT* denotes a global slowing of the motion, which is mainly due to the decrease in the linear stiffness C_{10}. However, the results of the previous section show that this effect is enhanced by the changes in motion topology: For the highest *ID*, the linear stiffness is minimal, while the softening spring behavior is maximal. The major consequence of this is an increased dwell time at the targets for higher difficulties.

To adapt to the accuracy constraints of the task, the system must change the coefficients of the damping function, which acts mainly on the spatial aspects of the behavior. The dissipative linear damping coefficient C_{01} increased when target width decreased without a significant effect of distance and no interaction (Fig. 7C). Hence, the stability of the limit cycle attractor increased with the absolute precision requirements (significant linear regression with $r^2 = 0.84$, $F(1,23) = 128.06$, $P < 0.0001$), while the distance to be covered had little influence on the stability of the system. It is important to note that this result can be considered a simple redescription (in the language of the equation parameters) of the absolute precision constraint at the level of the task definition: A narrower target requires more stable

Table 2. Results of the ANOVA on the coefficients of the RD model in absolute time and space. For each experimental factor, the *F* value and *ES* of the effect is reported. The significance of the *F* values was determined after Greenhouse and Geiser correction ($P < 0.05$) (*MT* movement time)

	Target width effect		Distance effect		Interaction D*W		ID effect	
	$F(4,32)$	ES (%)	$F(4,32)$	ES (%)	$F(16,128)$	ES (%)	$F(17,136)$	ES (%)
C_{10}	16.60	15.47	25.55	24.3	1.94[a]	4.13	11.83	50.21
C_{30}	12.23	9.75	22.28	30.23	8.34	15.43	4.12	26.22
C_{01}	35.85	43.48	2.60[a]	1.79	1.86[a]	3.60	12.47	49.33
C_{03}	26.27	36.07	6.63	4.78	8.86	19.22	12.48	55.31
MT	126.20	67.20	72.84	14.67	2.39[a]	1.48	56.46	85.82

[a] Nonsignificant *F* value ($P > 0.05$)
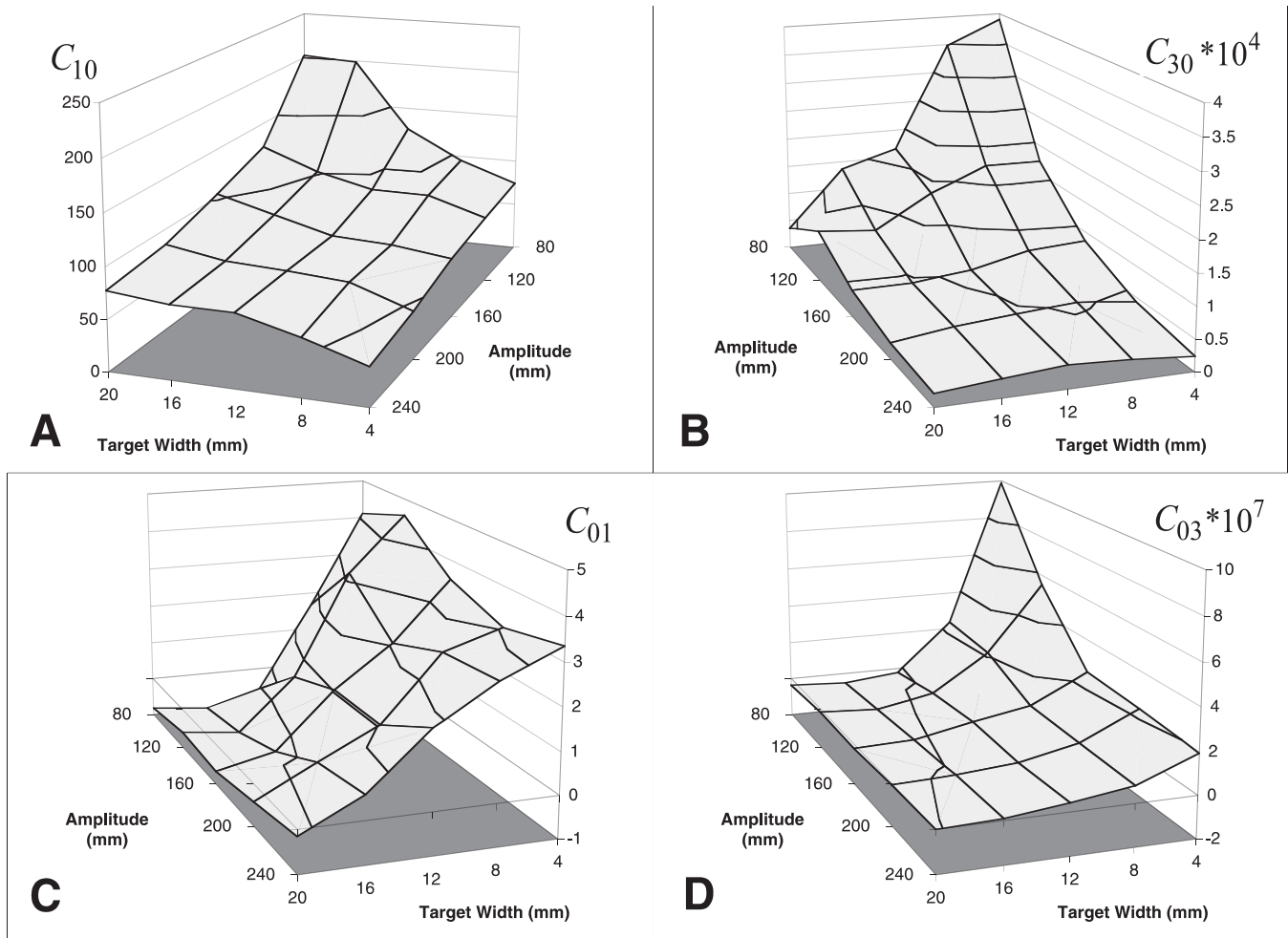
Fig. 7A–D. Landscape representation of the RD model's coefficients in real time and space metrics as a function of distance and target width: **A** linear stiffness coefficient C_{10}, **B** cubic Duffing stiffness coefficient C_{30}, **C** linear damping coefficient C_{01}, **D** cubic Rayleigh damping coefficient C_{03}

behavior, hence a higher linear damping coefficient C_{01}. The cubic damping coefficient C_{03} was also found to increase with target width and distance, with a significant interaction (Fig. 7D). Because the cubic damping coefficient C_{03} has little meaning when considered in isolation,[3] the latter result is difficult to interpret.

We can conclude that all the nonlinear components included in the RD model are important to capture the behavior in rhythmical aiming. The general increase of the nonlinear terms with task difficulty implies an increase in both nonlinear stiffness and damping which adequately reproduce the nature of the task constraints. Summarizing the main results of the present study, one can argue that the spatial accuracy constraints are accommodated by changes in the damping (mainly a more attractive limit cycle for narrower targets), while the time constraints are accommodated by changes in the stiffness function (most notably a local decrease in stiffness). In this context, the time/accuracy constraints

are accommodated through a subtle relation between damping and stiffness: The nonlinear Duffing stiffness leads to an increasing dwell time near the targets when necessary for high levels of task difficulty, which ensures that the (local) relaxation time is kept smaller than the (half)-cycle time. This, in turn, allows the task to be performed with an adequate error rate while keeping the overall movement frequency as high as possible. This interpretation deserves further empirical testing through perturbation experiments.

6 Discussion

The aim of the present article was to address the question: What is the attractor underlying goal-directed rhythmic aiming movements?

Seeking for a model combining a minimal number of terms in the equation of motion, we have shown that a dynamical model combining Rayleigh and Duffing terms can capture the main kinematic features of performance on a rhythmical Fitts' task. The modeling strategy and assumptions which led to the RD model are that of the W method (Beek and Beek 1988), with an emphasis on

---

[3] In the RD model, the amplitude of the limit cycle results from nontrivial interactions between the cubic damping term (which acts as a constraint on the maximal velocity) and the stiffness function (which can be far from linear).

the graphical analysis to qualitatively derive the oscillatory components and a subsequent statistical analysis to quantify the contribution of these components. However, the minimality criterion in our modeling strategy raises two problems, each of which can be addressed at the price of including new terms in the stiffness and damping definitions.

First, with a cubic softening spring stiffness, the system described by the RD model diverges to infinity when the position reaches a root of the stiffness function. Obviously, this behavior is not representative of real world motion because it would imply, for example, the inability to manage any overshoot. This problem can easily be dealt with through the inclusion of a quintic Duffing term in (4). With a quintic Duffing term added, the stiffness potential function can exhibit local minima in the neighborhood of the targets (e.g., Gonzalez and Piro 1987). Hence, including a quintic Duffing term in the RD model allows a stable behavior both within and outside the inter-root interval.

Second, when ID was low, the RD model led to unrealistic unstable oscillations, indicating that amendments are needed for the damping description. It is important to recall that, because Rayleigh is velocity-driven and Van der Pol position-driven, they act orthogonally in phase space. Their effect on the skewness of the limit cycle is inverted, as is their effect on the asymmetry in Hooke's plane. Changing Rayleigh for Van der Pol dissipation in our modeling gave rise to a systematic sign reversal for the linear and nonlinear dissipative terms: The Van der Pol-based model produced stable limit cycles for ID lower than 4, but unstable limit cycles for ID above 4. As a consequence, a stable realistic model should exhibit Rayleigh dissipation (for a high ID) and Van der Pol dissipation (for a low ID). We face here a limit in the power of the analysis with our statistical method. Because Van der Pol and Rayleigh terms act as sine and cosine skewing on the circular phase trajectory of an harmonic process, their combined influence can lead to a perfectly harmonic graphical representation (circular phase trajectory and linear Hooke's plane) in the presence of strong but equal Rayleigh and Van der Pol coefficients. Our graphical and statistical method can only assess the sum (difference) of the combined influence of Rayleigh and Van der Pol terms. Hence, the results reported here show that (i) Van der Pol was stronger than Rayleigh for low IDs and that (ii) Rayleigh became more important than Van der Pol when ID increased. To gain more insight into the dissipative oscillator components, methods that are more powerful are needed to directly assess the stability of the behavior as in perturbation experiments (Eisenhammer et al. 1991).

The conclusion to be drawn here is that, for general stability reasons and even if the model complexity increases, a realistic model of Fitts' task should include (i) a quintic term in the Duffing stiffness definition and (ii) a hybrid Van der Pol plus Rayleigh damping. The price to pay with the inclusion of these new terms in the model is that a precise assessment of the coefficients is no longer possible using the W method.

In the literature, a number of studies are reported in which the kinematics observed in rhythmical movement of the upper arm are also modeled as limit cycles. Most of these studies addressed more or less directly the problem of the relations between time and space behavior, which is central to Fitts' task.

One modeling strategy has been to assume that stiffness is linear (and acts as a control parameter) and to rely on the analysis of the relations between frequency and amplitude or peak velocity to derive the damping function. Following such a strategy, Kay et al. (1987) proposed the so-called 'hybrid model' which combines nonlinear Raleigh and Van der Pol damping. More recently, a derived version with a frequency-dependent Rayleigh term was shown to better account for individual data (Beek et al. 1996). These models adequately capture the observed behavioral changes when frequency is increased in rhythmical movements without spatial constraints (i.e., drop of amplitude and increase of peak velocity in single-effector tasks, switch from antiphase to inphase coordination in bimanual tasks). The same relations between peak velocity, amplitude and frequency are observed in Fitts' task, hence justifying the importance of both Van der Pol and Rayleigh damping in this context (Schmidt et al. 1995).

However, to extend the results of these studies to the domain of spatially constrained rhythmical movements, nonlinear stiffness terms need to be included in the oscillator. In the present study, a Duffing term became manifest as a function of the spatial constraints on the task. With the W method, Beek et al. (1995) showed that the dynamical modeling of pendulum swinging implied the inclusion of nonlinear Duffing and π-mix (xx^2) stiffness terms together with nonlinear damping combining Van der Pol and Rayleigh terms. In their experiments, the relative and absolute contribution of the different terms varied as a function of the moment of inertia and amplitude of oscillation and as a function of the ratio of the actual frequency to the pendulum's eigenfrequency. One important aspect of this contribution was to unambiguously introduce the idea that nonlinear stiffness was an omnipresent component of pendulum swinging, while confirming the previous results on the presence of a hybrid Van der Pol and Rayleigh damping. Moreover, an important prediction and result from their experiment 3 was the presence of π-mix oscillators when 'precise points at which the movement has to come to rest are prescribed' (p. 506), which is precisely the case in Fitts' task. Our experimental data clearly confirm the presence of Rayleigh (possibly combined with Van der Pol) and Duffing terms, but the π-mix terms did not appear as clear components, either in the portraying of our data or in stepwise regressions including the π-mix terms. Consequently, the most common terms in dynamical modeling of upper arm movements appear to be the hybrid Van der Pol plus Rayleigh damping to which a nonlinear Duffing stiffness is added.

This result is important because the behavioral capabilities of such a model might extend far beyond the scope of rhythmical aiming. In a contribution aimed at dynamically modeling discrete movements, Schöner

(1990) used an analytically solvable nonlinear oscillator (that we denote GP oscillator) whose behavior has been extensively studied (Gonzalez and Piro 1987). One important aspect of this contribution is that the multiple dynamical regimes in the GP oscillator allow us to qualitatively reproduce the main types of human movement (i.e., postural, rhythmical, and discrete) using a single dynamical model. The behavioral capabilities of Schöner's model rely on the bifurcations in the GP oscillator. First, a Hopf bifurcation due to the nonlinear (Van der Pol) damping explains the switch from a point attractor to a limit cycle attractor. Second, a pitchfork bifurcation due to the nonlinear (Duffing) stiffness explains the switch from a single to a dual-point attractor. In such a context, discrete movements appear as a special case of rhythmical motion where a limit (half)-cycle serves to link two stable points. Schöner (1990) showed that coupling two such oscillators captured the synchronization properties of two-armed movements and, more importantly in the context of the present study, that the linear relation linking MT and amplitude qualitatively reproduced Fitts' law (when excluding the precision requirement from consideration). However, the model of Schöner (1990) is based on Van der Pol damping, which implies that peak velocity is always reached in the second half of the trajectory, thus leading to unrealistic velocity profiles for *ID*s higher than 4.

When comparing the oscillator components in the RD and GP models, the differences appear in the damping (Rayleigh or Van der Pol) and in the stiffness definition, which is quintic in the model used by Schöner (1990). Importantly, Hopf and pitchfork bifurcations are possible in both models (i.e., due to the Rayleigh damping and Duffing stiffness in the RD model). This similarity makes the dynamical regimes in the RD model similar to that of the GP oscillator, while being far more difficult to assess because the RD model is not exactly solvable. Even though this point deserves more mathematical and empirical attention, an important aspect of the RD model is that it offers the same behavioral capabilities as Schöner's model, while leading to more realistic kinematics.

Thus, a first conclusion is that a comprehensive model of human movements should allow for one or two stable points in the workspace, linked by a limit cycle. In dynamical modeling terms, these constraints act on the stiffness (which should be a quintic Duffing) and on the damping (which should combine Rayleigh and Van der Pol dissipation). Although this kind of model can capture most human behavior, it may become unwieldy in terms of its free parameters. However, it is worth noting that, in practice, modeling of human aiming movements might reduce to only a few stiffness and damping parameters and may reduce to even less when attention is paid to the relations between the parameters. This latter point is an important new route to investigate. Finally, a second conclusion is that our choice to address the problem at the level of the attractor allowed us to find that the behavior relies on the same dynamics whatever the task's difficulty. However, the normalized average cycles that served as the database for the analyses focus

on the attractor only. A next step would be to address the (half) cycle by cycle behavior, which could allow addressing the problem of variability in human motor behavior from a new perspective. Once the attractor is identified, the behavior around the attractor should allow description and quantification of what the noise in the system is and how it participates in the actual behavior.

References

Atkeson CG, Hollerbach JM (1985) Kinematic features of unrestrained vertical arm movements. J Neurosci 5:2318–2330

Beek PJ (1989) Juggling dynamics. Free University Press, Amsterdam

Beek PJ, Beek WJ (1988) Tools for constructing dynamical models of rhythmic movement. Hum Mov Sci 7:301–342

Beek PJ, Schmidt RC, Morris AW, Sim MY, Turvey MT (1995) Linear and nonlinear stiffness and friction in biological rhythmic movements. Biol Cybern 73:449–507

Beek PJ, Rikkert WEI, Van Wieringen PCW (1996) Limit cycle properties of rhythmic forearm movements. J Exp Psychol Hum Percept Perf 22:1077–1093

Bingham GP, Schmidt RC, Turvey MT, Rosenblum LD (1991) Task dynamics and ressource dynamics in the assembly of coordinated rythmic activity. J Exp Psychol Hum Percept Perf 17:359–381

Buchanan JJ, Kelso JAS, Guzman GC de (1997) Self-organisation of trajectory formation. I. Experimental evidence. Biol Cybern 76:257–273

Cremers J, Hübler A (1987) Construction of differential equations from experimental data. Z Naturforsch 42a:797–802

Eisenhammer T, Hübler A, Packard N, Kelso JAS (1991) Modeling experimental time series with ordinary differential equations. Biol Cybern 65:107–112

Fitts PM (1954) The information capacity of the human motor system in controlling the amplitude of movement. J Exp Psychol 47:381–391

Gonzalez DL, Piro O (1987) Global bifurcations and phase portrait of an analytically solvable nonlinear oscillator: relaxation oscillations and saddle-node collisions. Phys Rev A 36:4402–4410

Guiard Y (1993) On Fitts' and Hooke's laws: simple harmonic movement in upper-limb cyclical aiming. Acta Psychol 82:139–159

Haken H, Kelso JAS, Buntz H (1985) A theoretical model of phase transitions in human movements. Biol Cybern 51:347–356

Kay B, Saltzman EL, Kelso JAS, Schöner G (1987) Space-time behavior of single and bimanual rhythmical movements: data and limit cycle model. J Exp Psychol Hum Percept Perf 13:178–192

Kay B, Saltzman EL, Kelso JAS (1991) Steady-state and perturbed rhythmical movements: a dynamical analysis. J Exp Psychol Hum Percept Perf 17:183–197

Kelso JAS (1995) Dynamic patterns. The self-organization of brain and behavior. MIT Press, Cambridge, Mass

Kugler PN, Turvey MT (1987) Information, natural law, and the self-assembly of rhythmic movements. Erlbaum, Hillsdale

MacKenzie CL, Marteniuk RG, Dugas C, Liske D, Eickmeier B (1987) Three dimensional movement trajectories in Fitts' task: implications for control. Q J Exp Psychol [A] 39:629–647

Meyer DE, Abrams RA, Kornblum S, Wright CE, Smith KJE (1988) Optimality in human motor performance: ideal control of rapid aimed movements. Psychol Rev 95:340–370

Mitra S, Riley MA, Turvey MT (1997) Chaos in human rhythmic movement. J Motor Behav 29:195–198

Mottet D (1994) Approche dynamique du conflit vitesse-précision. Unpublished doctoral dissertation, Université d'Aix-Marseille, Marseille, France

Mottet D, Bootsma RJ (1995) A dynamical model for Fitts' task. In: Bardy BG, Bootsma RJ, Guiard Y (eds) Studies in perception and action III. Erlbaum, New York, pp 91–94

Plamondon R, Alimi AM (1997) Speed/accuracy trade-offs in target-directed movements. Behav Brain Sci 20:279–349

Saltzman EL, Kelso JAS (1987) Skilled actions: a task-dynamic approach. Psychol Rev 94:84–106

Schmidt RC, Corey D, Fitzpatrick P, Riley M (1995) The oscillatory basis of Fitts' Law. In: Bardy BG, Bootsma RJ, Guiard Y (eds) Studies in perception and action III. Erlbaum, New York, pp 95–98

Schöner G (1990) A dynamic theory of coordination of discrete movement. Biol Cybern 63:257–270

Schöner G, Kelso JAS (1988a) Dynamic pattern generation in behavioral and neural systems. Science 239:1513–1520

Schöner G, Kelso JAS (1988b) A dynamic pattern theory of behavioral-change. J Theor Biol 135:501–524

Woodworth RS (1899) The accuracy of voluntary movement. Psychol Rev 3:1–106

Zaal FTJ, Bootsma RJ (1995) The topology of limb deceleration in prehension tasks. J Motor Behav 27:193–207